Section 6

Developments in global forecast models, case studies, predictability investigations, global ensembles.

CURRENT STATUS AND FUTURE PLANS FOR THE CPTEC GLOBAL ENSEMBLE PREDICTION SYSTEM

Carlos Frederico Bastarz[1], José Paulo Bonatti[1], Luiz Fernando Sapucci[1] and Silvio Nilo Figueroa[1]

[1]Center for Weather Forecasts and Climate Studies, National Institute for Space Research, Cachoeira Paulista, São Paulo, Brasil

e-mail: carlos.bastarz@inpe.br

1. Introduction

The CPTEC global Ensemble Prediction System (EPS) was implemented operationally for extended weather predictions at the beginning of the year 2000. This system makes use of the Empirical Orthogonal Functions (EOF) for the perturbation of a deterministic high-resolution control initial condition provided by NCEP. Over the years, the CPTEC global EPS was applied in several research investigations and was subject to improvements and updates. The most important update was perturbation of new variables in target regions. These improvements allowed the CPTEC global EPS to run in operational mode providing extended global weather forecasts (up to 15 days). CPTEC participated in the THORPEX/TIGGE project, thus its EPS has a global visibility and was used in comparison and validation studies along with EPSs of several other providers, like NCEP, CMC, ECMWF, KMA, JMA and MetOffice. The last developments at the TIGGE participating centers regarding the global EPS technique for numerical weather prediction include the application of coupled systems and data assimilation, which allows the perturbations to be updated at each analysis cycle using an ensemble of forecasts in a hybrid method. CPTEC has plans to upgrade its global EPS and is already working in this direction. A review of its current status is given as well as a future perspective envisioning new developments and the demands from the scientific community.

2. Current Status of the CPTEC Global Ensemble Prediction System

In its current version, the CPTEC global EPS uses an improved version of the EOF based perturbation technique, which includes perturbations for the surface pressure, horizontal wind components, specific humidity, and air temperature. These perturbations are applied over the Northern/Southern Hemispheres, the Tropical region and the north and south portions of South America (Mendonça and Bonatti, 2009; Cunningham et al., 2015). Figure 1 shows an example of the Continuous Rank Probability Skill Score for the air temperature at 850 hPa of the current version (oensMB09) in comparison with the previous version (oens_MCGA) and a new test one (oensMB09_mcga4.0).

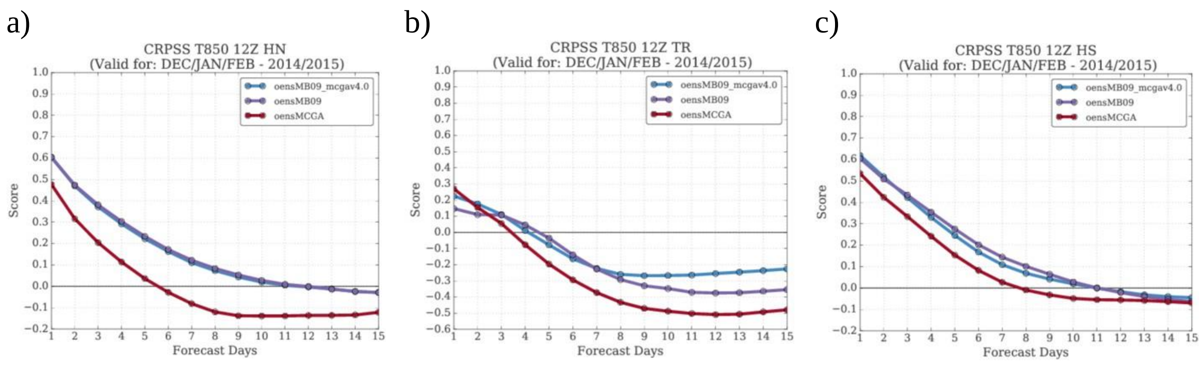

Figure 1. Continuous Rank Probability Skill Score for three different global EPS experiments, using the global circulation model from CPTEC. The oensMB09_mcga4.0 refers to the new CPTEC global EPS with the BAM model (Figueroa et al., 2016), the oens_MB09 refers to the current setup (as of April 2016) of the operational EPS system at CPTEC and the oens_MCGA refers to the previous version (as reported in Hagedorn et al., 2012).

3. Future Plans for the CPTEC Global Ensemble Prediction System

As CPTEC is making plans to move its global data assimilation system towards a hybrid 3DVar, an evolution to its global ensemble prediction system can also be envisioned. Currently, the CPTEC global EPS for extended range is not coupled with any other system (e.g., land-surface or ocean models). In terms of data assimilation, as CPTEC is updating its operational atmospheric data assimilation system, a land-surface data assimilation scheme is also in test to provide updates to the soil moisture conditions used within the BAM model (Figueroa et al., 2016) analysis. A hybrid 3DVar system was already successfully tested with the BAM model and is based on an Ensemble Kalman Filter (EnKF) system to draw the ensemble covariances. Some experiments were made in order to test the ability of this new system to provide a continuous ensemble of analysis for the extended range numerical weather prediction. Although the system was successfully run in a TQ0062L028 model resolution, it was found that a proper choice of the system configuration was needed to achieve at least the same ensemble system performance as using the EOF based perturbation (as shown in Figure 1). This upgrade in the global EPS for CPTEC is under investigation and will be released in the next years. As a main advantage, the upgraded system will benefit of a modern modeling framework in which a data assimilation system will be used to provide the model analysis.

A complete evaluation of the current system is published as an internal report at the National Institute for Space Research (INPE). For the near future, CPTEC has plans to upgrade the model version of the EPS, using the same version that is in use for the deterministic forecast (as reported in Figueroa et al. 2016). This upgrade will also carry an increase in the model horizontal/vertical resolution to TQ00213L042 (roughly 60 km near the Equator). As CPTEC global EPS is moving to a new model version and resolution other minor improvements are being made to the system related to bug corrections and adjustments in the perturbation method. As soon as an initial validation of this new system version is complete, a specific report will be made in order to show the complete system progress to the THORPEX community.

References

Bastarz, C.F., L.F. Sapucci, J.P. Bonatti, and L.G.G. Gonçalves, 2016: **Sistema de Modelagem por Conjunto (SMC) (Versão Inicial V0.0). Ensemble Prediction System (EPS) (Initial Version v0.0).** São José dos Campos: INPE, 98 p. in Portuguese. Disponível em: <http://urlib.net/8JMKD3MGP3W34P/3M9Q9K5>.

Cunningham, C., J.P. Bonatti, and M. Ferreira, 2015: **Assessing Improved CPTEC Probabilistic Forecasts on Medium-Range Timescale**. Meteorological Applications 22 (3): 378–384. issn: 1469-8080. doi:10.1002/met.1464.

Figueroa, S.N., J.P. Bonatti, P.Y. Kubota, G.A. Grell, H. Morrison, S.R. Barros, J.P. Fernandez, E. Ramirez, L. Siqueira, G. Luzia, J. Silva, J.R. Silva, J. Pendharkar, V.B. Capistrano, D.S. Alvim, D.P. Enoré, F.L. Diniz, P. Satyamurti, I.F. Cavalcanti, P. Nobre, H.M. Barbosa, C.L. Mendes, and J. Panetta, 2016: **The Brazilian Global Atmospheric Model (BAM): Performance for Tropical Rainfall Forecasting and Sensitivity to Convective Scheme and Horizontal Resolution.** Wea. Forecasting, 31, 1547–1572.

Hagedorn R., R. Buizza, T.M. Hamill, M. Leutbecher and T.N. Palmer, 2016: **Comparing TIGGE multimodel forecasts with reforecast-calibrated ECMWF ensemble forecasts**. Quarterly Journal of the Royal Meteorological Society V. 138, N. 668, Pages 1814-1827.

Mendonça, A.M., and J.P. Bonatti, 2009: **Experiments with EOF-Based perturbation methods and their Impact on the CPTEC/INPE Ensemble Prediction System.** São José dos Campos: Instituto Nacional de Pesquisas Espaciais.

Investigation of Radiative Effects of Atmospheric and Dust Aerosols Using a Modified Global Spectral Model and Its Impact on the Atmospheric Environment and Climate

Z.N. Begum

Ex-Scientist 'G'/Advisor, Department of Science and Technology, New Delhi, India and OWSD Full member, Trieste, Italy

(Email: begumzn@hotmail.com)

Abstract

The 'Atmospheric Global Spectral Model' with modified physical parameterization considering atmospheric and dust aerosols is used to predict radiative fluxes over the deserts and adjoining region of the Indian subcontinent and the Arabian Peninsula. The background field of sand soil and dust aerosol particles are considered in the arid and semi-arid regions over the globe. Using the modified model, the radiative fluxes and change in the global temperature has been computed. The radiative heating due to atmospheric and dust aerosols contribute major energy source on the radiative forcings and global energy balance. It is found that the model-derived values for change in temperature over the globe increases gradually year after year which may lead to global climate change.

Keywords: Radiative forcings , Aerosols, Modified AGCM, Environment and Climate

1. Introduction

The dry hot desert and the summer meteorological conditions provide ideal conditions creating dust storms. Heat waves, generally known as 'loo' in India, are frequent in the months of May-June, before the onset of monsoon. The dust outbreak is one of the major phenomena that occurs over the desert of Saudi Arabia during the summer, which influences the nearby areas of Arabian peninsula and the Arabian sea. The 'shamal', a strong northwesterly wind-flow causes the major dust storm over Saudi Arabia. The aerosols and dust absorb a part of the incoming shortwave radiation and reflect/scatter the remaining portion of the radiation. The radiative effect and climate impact of aerosols is one of the major uncertainties in the radiative forcing of climate change.

2. Modeling Aspects

The details of the Atmospheric Global Spectral Model (also known as 'Atmospheric Global Circulation Model'AGCM-O is originally adapted from NMC, U.S.A. The details of the model are discussed by Kanamitsu (1989). However, in the modified model AGCM-M, we have implemented the modified parameterization scheme (Begum (2003), (1998), (2017); Begum and George (1999)) where atmospheric aerosols including dust aerosols have been considered. For the identification of desert, semi-desert and short-grass regions, the land cover data, as reported by Ackerman et al. (1989) are used in this work.

The surface radiation balance can be expressed in the form of budget equation composed of different terms, each representing a radiation transport or conversion process,

$$QNET = QSW + QLW$$

where QNET is the net all wave radiation, QSW represents the net short wave radiation (incoming and outgoing), and QLW is the net long wave radiation.

3. Results and discussion

The change of temperature derived from the present modified model AGCM-M for the years 1995 - 2002 is depicted in Fig.1 and is validated with the results of Hansen et al. (2000a, 2000b) using AGCM-O. Both the results show a gradual increase in temperature change over the said years, which contribute to global warming.

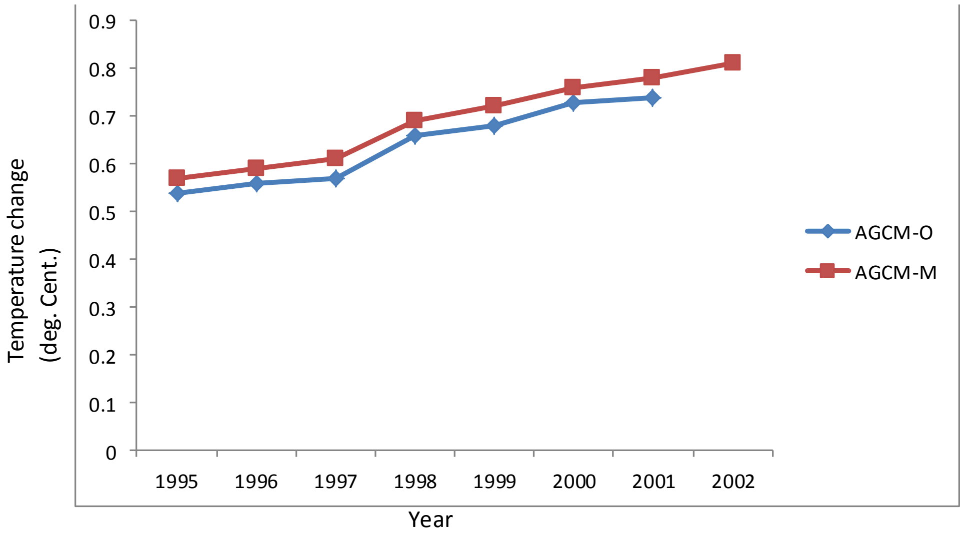

Fig.1. Plot of the change of temperature derived from the present modified model (AGCM-M) for the years 1995-2002 and its validation with AGCM-O.

4. Conclusions

The radiative effect and the climate impact of the atmospheric and dust aerosols is one of the main uncertainties in the radiative forcing of climate change. To minimize such uncertainties, our modified global circulation model (AGCM-M) incorporates more realistic physical parameterization, which successfully explains the radiative fluxes and rise in the global temperature.

References

Ackerman SA, Cox SK (1989) Surface weather observations of atmospheric dust over the Soutwest Summer monsoon region. Meteorol Atmos Phys 41: 19-34.

Begum ZN (1998) Scattering of solar radiation by aerosol particulates in the atmosphere: a theoretical approach validated with pre- INDOEX. J Atmos Sol-Terr Phys 60: 1751-4.

Begum ZN, George JP (1999) Significance of mineral dust aerosols in the global atmospheric model radiative forcings: results validated with Pre-INDOEX. Acta Geophys Polon XLVII: 231-235.

Begum ZN (2003) A theoretical investigation of the radiative effects and microphysical processes involved in the interaction of aerosol particulates in the atmosphere and validation of the theoretical results with INDOEX observations. J Quant Spect Rad Trans 78: 99-103.

Begum ZN (2017) The Effect of Radiative Forcings of Various Constituents of the Earth Atmosphere on the Global Energy Transfer. In: Astakhova E (ed) WCRP Report No. 12/2017 on World Climate Research Programme - Research Activities in Atmospheric and Ocean Modeling, Section 4.

Hansen JE, Sato M, Ruedy, Lacis A, Oinas V (2000a) Global warming in the twenty –first century an alternative scenario. Pro. Natl Acad Sci 97: 9875-9880.

Hansen JE, Ruedy R, Sato M, Lo K (2000b). Global warming continues. Science 295 (Issue: 5553): 275.

Kanamitsu M (1989) Description of the NMC global data assimilation and forecast system. Weather and Forecasting 4: 335-342.

The global ICON Ensemble

M. Denhard, A. Rhodin, H. Frank, H. Anlauf, C. Primo, L. Kirchhuebel, M. Paulat, A. Fernandez del Rio, A. Cress, J. T. Ambadan, G. Zängl, R. Potthast, M. Buchhold

Deutscher Wetterdienst (DWD), Offenbach, D-63067, Germany
email: michael.denhard@dwd.de

The ICOsahedral Non-hydrostatic general circulation modelling framework (ICON) has been jointly developed by the Max Planck Institute for Meteorology in Hamburg and the German Weather Service (Zaengl et al., 2014). It is based on a triangular grid with nearly uniform resolution on the globe which enables local refinements by two-way grid nesting. The global ICON forecast suite at DWD became operational in January 2015. The deterministic configuration has 90 vertical layers and a global horizontal resolution of 13km including a two-way nested 6.5km (60 layers) refinement over Europe.

Based on the ICON modelling framework DWD runs an ICON ensemble suite with 40 members. In contrast to the deterministic system the horizontal resolution is approx. 40km on the global scale and 20km over Europe. Since 17th January 2018 the ICON-EPS runs 8 times a day in operational mode. At 03/09/15/21UTC the maximum lead time is limited to +30h. Otherwise, the European nest is integrated together with the global system up to +120h. For the 00/12 UTC runs the forecasts of the global system extend to +180h.

Perturbations in the ICON-EPS

The spread-skill properties of the ICON ensemble are mainly determined by the initial perturbations which are set by the global ensemble data assimilation system (EDA) running at DWD, because the ICON-EPS members are initialized directly from the EDA analysis states. The EDA is based on a Local Ensemble Transform Kalman filter (LETKF) implementation following Hunt et al. (2007) with a 3-hourly assimilation cycle. The algorithm solves the underlying equations in ensemble space spanned by a background ensemble of 40 members. The “Kalman gain” from adding observations may reduce the spread of the analysis ensemble and it must be re-inflated at each assimilation step. We use multiplicative inflation following Houtekamer et al. (2005) with a factor ranging from 0.9 to 1.5 and relaxation to prior perturbations (RTPP, Zhang et al., 2004) with a rate of 0.75. In addition, random perturbations are added to the analysis ensemble members, where the vertical correlations are estimated from the climatological background error co-variances determined by the NMC Method. Horizontal correlations are prescribed with a length scale of 400 km for geopotential, velocity potential and stream function and 200km for relative humidity. In addition, SST’s are perturbed by 1° K random perturbations with spatial correlations of 100km/1000km and correlations in time of one day. The flow-dependent error co-variances of the LETKF EDA are used in a further hybrid-variational analysis step (En-Var) to generate the high resolution analysis for the operational deterministic system (13km/6.5 km).

To simulate model error a simple methodology for perturbing various physics tuning parameters has been implemented. At the beginning of each forecast the actual values of a predefined set of tuning parameters are calculated using a random number generator depending on the ensemble member ID. The user can specify a range within each parameter may vary. For most parameters, the perturbation is applied in an additive symmetric way by setting pert_param = ref _param + 2*(rand_num - 0.5)*range, where rand_num = [0; 1]. The perturbations remain constant during the forecast. A list of perturbed tuning parameters can be found in the “ICON Database Reference Manual” at www.dwd.de.

Evaluation

A subjective evaluation (see Figure 1) during summer 2017 by the forecasters at DWD shows that in the majority of relevant wind gust events (upper panels) the ICON-EPS adds value to the existing warning process. For precipitation (lower panels) this effect is less pronounced but still noticeable. In general, the added value is larger for the short range (0-48h) than for the early medium range (60-108h). Because the latter time period is somewhat longer than the former, we observe more cases in the latter period (e.g. 479 vs. 604 cases for the wind gusts). An objective verification with more recent data is in preparation (Denhard et. al. 2018).

wind gust (6h)

0-48h

		479 cases	%
added value	Yes	285	59,5
	some	121	25,3
	No	73	15,2

60-108h

		604 cases	%
added value	Yes	297	49,2
	some	175	29
	No	132	21,8

precipitation (12h)

		61 cases	%
added value	Yes	23	37,7
	some	15	24,6
	No	23	37,7

		91 cases	%
added value	Yes	20	22,0
	some	17	18,7
	No	54	59,3

Fig. 1: *Subjective verification of 6-hourly wind gusts (upper panel) and 12-hourly precipitation events which exceed the different warning thresholds used at DWD. The forecasters ranked the ICON-EPS forecast in three categories according to their added value for the alert generation process: yes, some or no added value. All cases are considered, where either an event was observed or forecasted by the ensemble with a likelihood of at least 10%. The evaluation has been done separately for the short (0-48h) and early medium (60-108) range in summer 2017.*

References

Denhard M, Rhodin A, Frank H, Anlauf H, Primo C., Fernandez del Rio A, Cress A, Ambadan J T, Zängl G, Potthast R, Buchhold M, 2018: The global ICON Ensemble at DWD. Deutscher Wetterdienst, Offenbach, Germany, in preparation.

Houtekamer P, Mitchell H, Pellerin G, Buehner M, Charron M, Spacek L, Hansen M, 2005: Atmospheric data assimilation with an ensemble Kalman filter: Results with real observations. Mon. Wea. Rev. 133(3): 604–620, doi:f10.1175/MWR-2864.1g

Hunt BR, Kostelich EJ, Szunyogh I. 2007. Efficient data assimilation for spatiotemporal chaos: A local ensemble transform kalman filter. Physica D: Nonlinear Phenomena 230(12): 112–126.

Zaengl G, Reinert D, Ripodas P, Baldauf M, 2014: The ICON (icosahedral non-hydrostatic) modeling framework of DWD and MPI-M: Description of the non-hydrostatic dynamical core. Q. J. R. Meteorol. Soc. 141: 563–579, January 2015 B DOI:10.1002/qj.2378.

Zhang F, Snyder C, Sun J, 2004: Impacts of initial estimate and observation availability on convective-scale data assimilation with an ensemble Kalman filter. Mon. Weather Rev. 132: 1238–1253. https://doi.org/10.1175/1520-0493(2004)132<1238:IOIEAO>2.0.CO;2.

Predictability of weather-climate anomalies in the North Eurasian regions during transitions from the La Niña conditions

I.I. Mokhov[1,2] and A.V. Timazhev[1]

[1]A.M. Obukhov Institute of Atmospheric Physics RAS
[2]Lomonosov Moscow State University
mokhov@ifaran.ru

The impact of the El Niño / La Niña events is significant on a global scale, including in the Russian regions (Mokhov, Timazhev, 2015). In (Mokhov, Timazhev, 2016) estimates of possible anomalies in Russian regions in 2016 in May-July are obtained, taking into account the beginning of the year in the El Niño phase and the forecasts of its transformation by the end of the year. Here we present similar estimations for 2018 with the beginning in the La Niña phase with negative anomalies of sea surface temperature (SST) in the east-central and eastern equatorial regions of the Pacific Ocean. According to early-April CPC/IRI official probabilistic ENSO forecast on the basis of ensemble model simulations the probability of the *L*-phase continuation to the end of 2018 is about 10%. The corresponding probabilities for *N*-phase and *E*-phase are about 40% and 50%, correspondingly.

We analyze the spring-summer (May-July) anomalies of surface air temperature (SAT) δT and precipitation δP, and also drought (*D*) and excessive moisture (*M*) indices for European (ER) and Asian (AR) parts of Russia in mid-latitudes from observations since 1891 from (Meshcherskaya et al., 2011). For estimation of the El Niño / La Niña effects, we used their indices characterized by the sea surface temperature (SST) in the Niño3, Nino3,4 and Nino4 regions in the equatorial latitudes of the Pacific Ocean. The El Niño (*E*), La Niña (*L*) and neutral (*N*) phases are defined similar to (Mokhov, Timazhev, 2015).

Table 1 shows the estimates for probability of spring–summer temperature anomalies δT in the ER for different transitions from the *L*-phase at the beginning of the year with the use of different indices.

Table 1. Probability of positive and negative surface air temperature anomalies (δT) in the ER (and AR) in May-July for different transitions from La-Nina conditions at the beginning of the year (characterized by indices Nino3, Nino3,4 and Nino4) from observations since 1891.

δT, K		**Nino3 *n*=29**			**Nino3,4 *n*=36**			**Nino4 *n*=28**		
		***L*→*E* *n*=7**	***L*→*L* n=9**	***L*→*N* n=13**	***L*→*E* *n*=11**	***L*→*L* *n*=14**	***L*→*N* *n*=11**	***L*→*E* *n*=4**	***L*→*L* *n*=10**	***L*→*N* *n*=14**
>0	**>0**	**4/7 (5/7)**	**3/9 (5/9)**	**5/13 (8/13)**	**6/11 (7/11)**	**5/14 (9/14)**	**7/11 (4/11)**	**2/4 (2/4)**	**4/10 (5/10)**	**6/14 (8/14)**
	>1K	**2/7 (1/7)**	**1/9 (2/9)**	**2/13 (3/13)**	**3/11 (2/11)**	**3/14 (3/14)**	**3/11 (4/11)**	**1/4 (1/4)**	**2/10 (2/10)**	**3/14 (4/14)**
≤0	**≤0**	**3/7 (2/7)**	**6/9 (4/9)**	**8/13 (5/13)**	**5/11 (4/11)**	**9/14 (6/14)**	**4/11 (6/11)**	**2/4 (2/4)**	**6/10 (5/10)**	**8/14 (6/14)**
	≤-1K	**2/7 (2/7)**	**0/9 (0/9)**	**2/13 (1/13)**	**2/11 (2/11)**	**1/14 (0/14)**	**0/11 (2/11)**	**0/4 (1/4)**	**1/10 (0/10)**	**1/14 (1/14)**

Table 2 shows corresponding estimates for probability of positive and negative precipitation anomalies (δP) in the ER (and AR) in May-July for different transitions from La-Nina conditions at the beginning of the year.

Table 2. Probability of positive and negative precipitation anomalies (δP) in the ER (and AR) in May-July for different transitions from La-Nina conditions at the beginning of the year.

δP **[%]**		**Nino3** ***n*=29**			**Nino3,4** ***n*=36**			**Nino4** ***n*=28**		
		***L→E n*=7**	***L→L*** **n=9**	***L→N*** **n=13**	***L→E n*=11**	***L→L n*=14**	***L→N n*=11**	***L→E n*=4**	***L→L n*=10**	***L→N n*=14**
<0	**<0**	**3/7 (4/7)**	**5/9 (5/9)**	**4/13 (4/13)**	**7/11 (5/11)**	**6/14 (5/14)**	**7/11 (3/11)**	**2/4 (3/4)**	**6/10 (5/10)**	**6/14 (5/14)**
	<-20%	**1/7 (2/7)**	**2/9 (1/9)**	**0/13 (1/13)**	**1/11 (2/11)**	**2/14 (1/14)**	**1/11 (1/11)**	**0/4 (1/4)**	**2/10 (1/10)**	**1/14 (2/14)**
≥0	**≥0**	**4/7 (3/7)**	**4/9 (4/9)**	**9/13 (9/13)**	**4/11 (6/11)**	**8/14 (9/14)**	**4/11 (8/11)**	**2/4 (1/4)**	**4/10 (5/10)**	**8/14 (9/14)**
	>20%	**0/7 (1/7)**	**0/9 (0/9)**	**1/13 (2/13)**	**0/11 (1/11)**	**0/14 (0/14)**	**1/11 (2/11)**	**0/4 (0/4)**	**0/10 (0/10)**	**1/14 (1/14)**

Table 3 shows corresponding estimates for probability of different drought (*D*) and excess moisture (*M*) conditions in the ER (and AR) in May-July for different transitions from La-Nina conditions at the beginning of the year.

Table 3. Probability of different drought (*D*) and excess moisture (*M*) conditions in the ER (and AR) in May-July for different transitions from La-Nina conditions at the beginning of the year.

D, M **[%]**		**Nino3** ***n*=29**			**Nino3,4** ***n*=36**			**Nino4** ***n*=28**		
		***L→E n*=7**	***L→L*** **n=9**	***L→N*** **n=13**	***L→E n*=11**	***L→L n*=14**	***L→N n*=11**	***L→E n*=4**	***L→L n*=10**	***L→N n*=14**
<0	**≥20%**	**2/7 (3/7)**	**2/9 (4/9)**	**3/13 (5/13)**	**4/11 (4/11)**	**4/14 (5/14)**	**6/11 (2/11)**	**1/4 (2/4)**	**3/10 (3/10)**	**4/14 (5/14)**
	≥30%	**2/7 (2/7)**	**2/9 (2/9)**	**2/13 (2/13)**	**3/11 (3/11)**	**4/14 (2/14)**	**3/11 (1/11)**	**1/4 (1/4)**	**3/10 (2/10)**	**3/14 (3/14)**
≥0	**≥20%**	**3/7 (2/7)**	**3/9 (0/9)**	**3/13 (3/13)**	**3/11 (2/11)**	**3/14 (0/14)**	**3/11 (3/11)**	**1/4 (2/4)**	**4/10 (1/10)**	**3/14 (4/14)**
	≥30%	**2/7 (1/7)**	**1/9 (0/9)**	**2/13 (0/13)**	**2/11 (1/11)**	**1/14 (0/14)**	**2/11 (0/11)**	**0/4 (0/4)**	**2/10 (0/10)**	**0/14 (2/14)**

This work was supported by the RFBR and RAS.

References

Meshcherskaya A.V., Mirvis V.M., Golod M.P. The drought in 2010 against the background of multiannual changes in aridity in the major grain-producing regions of the European part of Russia. *Tr. MGO,* 2011, **563**, 94–121 (in Russian)

Mokhov I.I., Timazhev A.V. Drought risk in the North Eurasian regions: Assessment of El-Nino effects. *Res. Activ. Atmos. Ocean. Modell.* E. Astakhova (ed.). WCRP Rep. No.12/2015, 2015, 2.6–2.7.

Mokhov I.I., Timazhev A.V. Weather-climate anomalies in Russian regions: El Niño-associated predictability. *Res. Activ. Atmos. Ocean. Modell.* E. Astakhova (ed.). WCRP Rep. No.15/2016, 2016, 6.9–6.10.

Verification of JMA's new GEPS for one-month prediction

Ryohei Sekiguchi, Yukimasa Adachi, Takafumi Kanehama, Yutaro Kubo,
Kengo Miyaoka, Akio Nishimura, Akihiko Shimpo, Takuma Yoshida
Climate Prediction Division, Japan Meteorological Agency, Tokyo, Japan
(E-mail: r_sekiguchi@met.kishou.go.jp)

1. Introduction

The Japan Meteorological Agency (JMA) replaced its previous One-month Ensemble Prediction System (EPS) (Hirai et al. 2014) with the Global EPS (GEPS) in March 2017 (Yamaguchi et al. 2018). The GEPS is an integrated system supporting JMA's issuance of typhoon forecasts, one-week forecasts, early warnings for extreme weather and one-month forecasts. This change includes major updates for the atmospheric forecast model and the method of generating initial and boundary perturbations (for details, see Yamaguchi et al. 2018). This paper outlines the performance of the GEPS verified in terms of one-month prediction via 30-year hindcast experiments.

2. Hindcast experiments

As specified in Table 1, the experiments were conducted for the 30-year period from 1981 to 2010 with atmospheric initial conditions produced from the Japanese 55-year Reanalysis (JRA-55; Kobayashi et al. 2015). Initial perturbations were created from a combination of initial singular vectors (SVs) and evolved SVs calculated using the SV method, while initial perturbations for the real-time system were produced by combining perturbations from the SV method and the Local Ensemble Transform Kalman Filter (LETKF) method (Yamaguchi et al. 2018). In these experiments, perturbations from the LETKF method were not adopted due to the high computational cost involved.

3. Verification results

With the weaker biases of velocity potential at 200 hPa over the Asian monsoon region in boreal summer, forecast mean errors of the GEPS are smaller than those of the previous One-month EPS (Figure 1). The four-week mean forecast fields of the GEPS also show smaller southward position biases for the sub-tropical jet stream than those of the previous One-month EPS (not shown).

For the anomaly correlation coefficients of geopotential height at 500 hPa over the Northern Hemisphere (20 – 90°N), the GEPS demonstrates improved forecast skill for most lead times and seasons (Figure 2).

Prediction skill for the Madden-Julian oscillation (MJO) is evaluated using the method described by Matsueda and Takaya (2012). As shown in Figure 3, the MJO amplitude of the GEPS is larger than that of the previous One-month EPS, but still smaller than that of analysis. Other MJO forecast skills (i.e., RMSE and correlation) of the GEPS are generally comparable to those of the previous One-month EPS (not shown).

Representation of quasi-biennial oscillation (QBO) is verified from the time series of equatorial zonal wind at 30 hPa (Figure 4). There is a large difference between the analysis (black line) and the forecast of the previous One-month EPS (blue lines), while the variation of zonal wind is better captured by the GEPS (red lines).

4. Summary

In this work, the one-month prediction performance of the GEPS was verified via hindcast experiments. Some of the major model biases seen in the previous One-month EPS were reduced, and the forecast skill of the GEPS was superior for most lead times and seasons. MJO amplitude and QBO representation were also improved.

Table 1 Hindcast experiment details

	Global EPS (GEPS)	Previous One-month EPS
Atmospheric forecast model	GSM1603 (Yonehara et al. 2017) with additional improvement of physical processes	GSM1304
Resolution (model top)	TL479L100 (0.01hPa) up to 18 days TL319L100 (0.01hPa) afterwards	TL319L60 (0.1hPa)
Period (initial date)	1981－2010 (10th, 20th, end of month)	
Ensemble size	5	
Initial perturbation method	Singular Vector (SV) method	Breeding of Growing Modes (BGM) method
Initial condition (atmosphere)	JRA-55	
Initial condition (land)	Calculated in advance using the land-surface model in the GEPS and atmospheric forcing from JRA-55	JRA-55
Verification data	JRA-55	

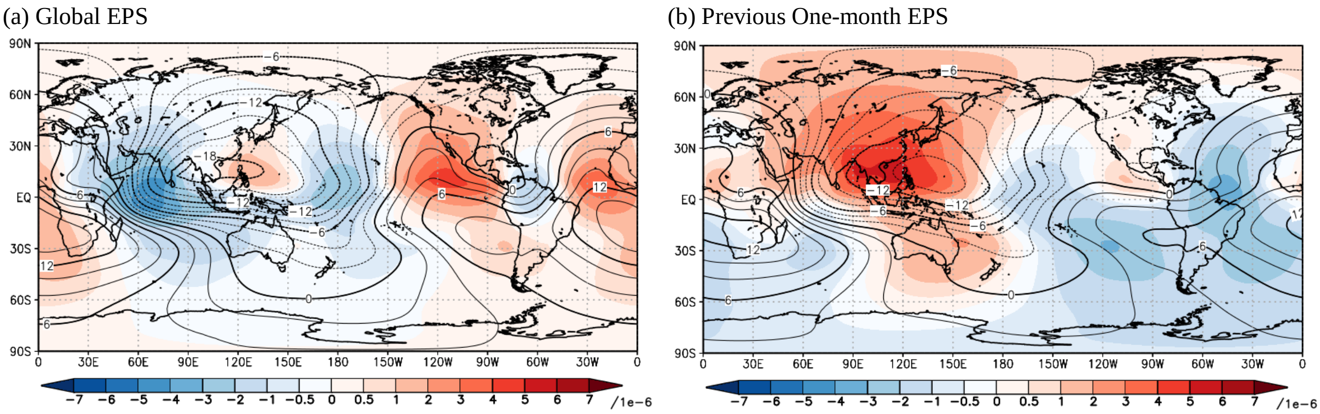

Figure 1 Climatological mean fields for 4-week mean (day 3 – day 30) velocity potential at 200 hPa (contours) and related mean errors (shading) for boreal summer with (a) the Global EPS (GEPS) and (b) the previous One-month EPS
The contour interval is 2×10^6 m^2/s.

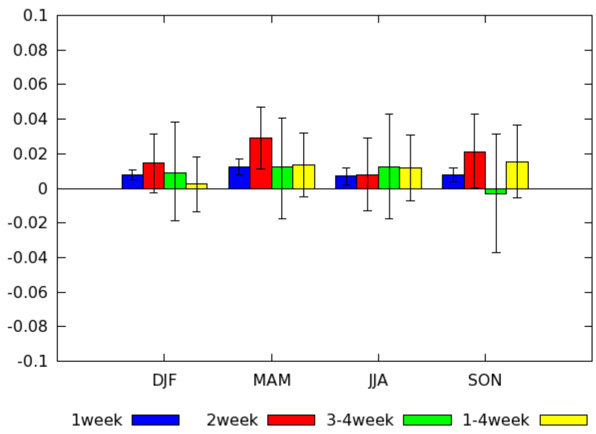

Figure 2 Differences in anomaly correlation coefficients for geopotential height at 500 hPa in the Northern Hemisphere (20 – 90°N) for all seasons
Positive values mean that anomaly correlation coefficients of the GEPS are larger than those of the previous One-month EPS. Error bars indicate the two-sided 95% confidence level.

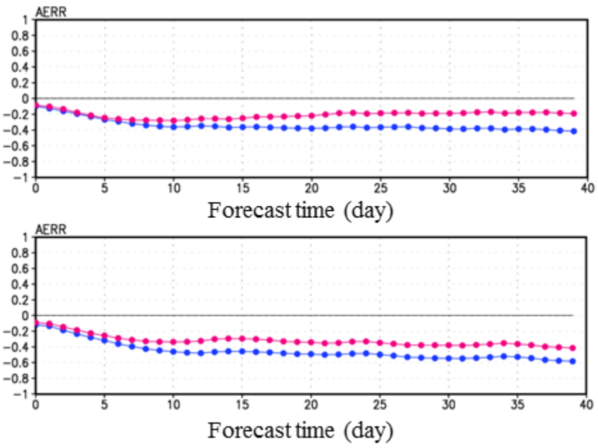

Figure 3 Mean MJO amplitude error for (top) boreal summer and (bottom) boreal winter
Positive (negative) values mean that the predicted MJO amplitudes are larger (smaller) than those of analysis. Blue and red lines represent results for the previous One-month EPS and the GEPS, respectively.

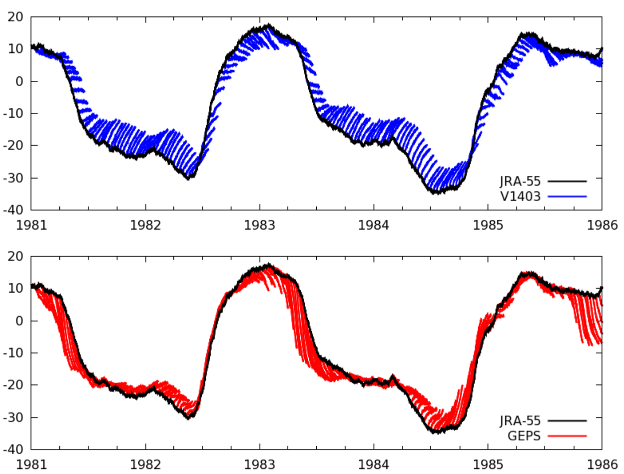

Figure 4 Time-series representation of equatorial (5°S – 5°N) zonal wind at 30 hPa (1981 – 1985)
Black lines represent analysis (JRA-55). Blue and red lines represent forecasts of the previous One-month EPS and the GEPS, respectively.

References

Hirai, M., K. Miyaoka, H. Sato, H. Sugimoto, A. Minami, and C. Matsukawa, 2014: March 2014 upgrade of JMA's One-month Ensemble Prediction System. *CAS/JSC WGNE Res. Activ. Atmos. Oceanic Modell.*, **44**, 6.09-6.10.

Kobayashi, S., Y. Ota, Y. Harada, A. Ebita, M. Moriya, H. Onoda, K. Onogi, H. Kamahori, C. Kobayashi, H. Endo, K. Miyaoka, and K. Takahashi, 2015: The JRA-55 reanalysis: General specifications and basic characteristics. *J. Meteor. Soc. Japan.*, **93**, 5-48.

Matsueda, S., and Y. Takaya, 2012: Forecast skill of MJO with the JMA's One-month Ensemble Prediction System. *CAS/JSC WGNE Res. Activ. Atmos. Oceanic Modell.*, **42**, 6.11-12.

Yamaguchi, H., D. Hotta, T. Kanehama, K. Ochi, Y. Ota, R. Sekiguchi, A. Shimpo, and T. Yoshida, 2018: Introduction to JMA's new Global Ensemble Prediction System. *CAS/JSC WGNE Res. Activ. Atmos. Oceanic Modell.*, submitted.

Yonehara, H., T. Tokuhiro, R. Nagasawa, M. Ujiie, A. Shimokobe, M. Nakagawa, R. Sekiguchi, T. Kanehama, H. Sato, and K. Saitou, 2017: Upgrade of parameterization schemes in JMA's operational global NWP model. *CAS/JSC WGNE Res. Activ. Atmos. Oceanic Modell.*, **47**, 6.17-6.18.

Introduction to JMA's new Global Ensemble Prediction System

Haruki Yamaguchi, Daisuke Hotta, Takafumi Kanehama, Kenta Ochi,
Yoichiro Ota, Ryohei Sekiguchi, Akihiko Shimpo, Takuma Yoshida
Japan Meteorological Agency, Japan
e-mail: h.yamaguchi@met.kishou.go.jp

1. Introduction

The Japan Meteorological Agency (JMA) put a new ensemble prediction system (EPS) called the Global EPS (GEPS) into operation in January 2017. Covering both medium- and extended-range forecasting, the system supports the issuance of five-day tropical cyclone (TC) forecasts, one-week forecasts, early warning information on extreme weather, and one-month forecasts. GEPS took over the roles of three previous JMA systems (the Typhoon EPS (TEPS; JMA 2017), the One-week EPS (WEPS; Yamaguchi et al. 2014) and the One-month EPS). The objectives of the integration were to utilize computational resources more effectively and to concentrate efforts into a single EPS system. TEPS and WEPS were replaced by GEPS in January 2017, and GEPS inherited the role of the One-month EPS in March 2017. Along with the introduction of GEPS, JMA also implemented an upgrade of the forecast model and an initial perturbation technique involving the Local Ensemble Transform Kalman Filter (LETKF; Hunt et al. 2007) and the singular vector (SV) method. A perturbation technique for sea surface temperature (SST) was additionally incorporated. This report gives an overview of GEPS with focus on TC track forecasting and one-week forecasting.

2. Global Ensemble Prediction System Specifications

Table 1 shows the specifications of GEPS and the previous TEPS, WEPS and One-month EPS systems. Parameterization scheme revisions include updating of treatments for land/sea surfaces, deep convection, cloud, gravity waves, boundary layers and radiation. The number of vertical layers was increased from 60 to 100, and the top-level pressure was changed from 0.1 to 0.01 hPa. SST perturbations were introduced, and LETKF was incorporated for revision of the initial perturbation production method.

The unperturbed initial condition is produced via interpolation of JMA's higher-resolution Global Analysis. SST and sea ice analysis is performed independently from the atmospheric initial condition and used as the lower boundary condition, which is then used to represent anomalies from the climatology. SST and sea ice anomalies at the initial time are fixed and added to the varying climatology during time integration.

Initial perturbations are generated using a combination of LETKF and SV. The ensemble spread based on perturbations from LETKF represents uncertainty in the initial conditions. SV-based perturbations are adopted to help ensure reasonable spreads for a medium-range lead time, and SST perturbations are designed to represent uncertainty in the prescribed SST. A stochastically perturbed physics tendency scheme is used in consideration of model uncertainties associated with physical parameterizations.

3. Impact of EPS Upgrade on TC Track Forecasting and One-week Forecasting

GEPS was examined for the period covering 2015 and 2016 to evaluate the results of TC track forecasting and one-week forecasting. As shown in Figure 1, the average TC track forecast errors of ensemble means determined using GEPS for the western North Pacific region were smaller than those determined using TEPS. As shown in Figure 2, Brier skill scores for probabilistic forecasts of 24-hour cumulative precipitation exceeding 1 mm over Japan during winter 2015/16 determined using GEPS were higher than those determined using WEPS. The upgrade of the forecast model significantly contributed to these improvements. The initial perturbation techniques of GEPS provide more appropriate distribution of initial spreads than the former system. Excessive initial perturbations in a limited area were observed with WEPS forecasts. The adoption of SST perturbations improves the spreads of atmospheric temperature over the ocean and large-scale convections in the tropics, but this improvement is unremarkable since other changes contribute more.

References

Hunt, B. R., E. J. Kostelich and I. Szunyogh, 2007: Efficient data assimilation for spatiotemporal chaos: a local ensemble transform Kalman filter. Physica. D., 230, 112 – 126.

Japan Meteorological Agency, 2017: Joint WMO Technical Progress Report on the Global Data Processing and Forecasting System and Numerical Weather Prediction Research Activities for 2016, JMA, p. 31 – 32.

Yamaguchi, H., M. Higaki and M. Kyouda, 2014: Upgrade of JMA's One-Week Ensemble Prediction System. CAS/JSC WGNE Res. Activ. Atmos. Oceanic Modell., 44, 6.17 – 6.18.

Table 1: Configurations of the current and previous systems. Bold red text represents major upgrades over the previous systems.

	Previous systems		Current system
Name	Typhoon EPS (TEPS) (before Jan. 2017)		Global EPS (GEPS)
	One-week EPS (WEPS) (before Jan. 2017)		
	One-month EPS (1 m) (before Mar. 2017)		
Main targets	TEPS	Typhoon forecasts	Typhoon forecasts, one-week forecasts, early warning information on extreme weather, one-month forecasts
	WEPS	One-week forecasts	
	1 m	Early warning information on extreme weather, one-month forecasts	
Frequency	TEPS	Up to 4 times a day	4 times a day (at maximum) when a TC is present, twice a day otherwise
	WEPS	Twice a day	
	1 m	4 times a week	
Forecast range (initial time)	TEPS	5.5 days (00, 06, 12, 18 UTC)	5.5 days (06, 18 UTC)*, 11 days (00, 12 UTC) except for 18 days (00, 12 UTC; Sat. & Sun.), 34 days (00, 12 UTC; Tue. & Wed.)
	WEPS	11 days (00, 12 UTC)	
	1 m	18 days (12 UTC; Sat. & Sun.) 34 days (12 UTC; Tue. & Wed.)	
Ensemble size	TEPS	25	27 up to 11 days, 13 thereafter
	WEPS	27	
	1 m	50 (25 x two consecutive initial times)	
Horizontal resolution	TEPS, WEPS	TL479 (approx. 40 km)	TL479 up to 18 days, TL319 thereafter
	1 m	TL319 (approx. 55 km)	
Vertical resolution (model top)	TEPS, WEPS, 1 m	60 levels (0.1 hPa)	**100 levels (0.01 hPa)**
Initial perturbations (targeted area)	TEPS	SV (western North Pacific, TC areas)	SV (Northern Hemisphere, Tropics, Southern Hemisphere) **+ LETKF**
	WEPS	SV (Northern Hemisphere, Tropics, Southern Hemisphere)	
	1 m	Breeding of Growing Modes (Northern Hemisphere, Tropics)	
Model ensemble	TEPS, WEPS, 1 m	Stochastically Perturbed Physics Tendency (SPPT)	
Boundary perturbations	TEPS, WEPS, 1 m	None	**Perturbations on SST**

* GEPS runs from base times at 06 and 18 UTC when any of the following conditions is satisfied:

- A TC of tropical storm (TS; defined as a TC with maximum sustained wind speeds of 34 knots or more and less than 48 knots) intensity or higher is present in the RSMC Tokyo - Typhoon Center's area of responsibility (0 – 60°N, 100°E – 180°).
- A TC is expected to reach TS intensity or higher in the area within the next 24 hours.
- A TC of TS intensity or higher is expected to move into the area within the next 24 hours.

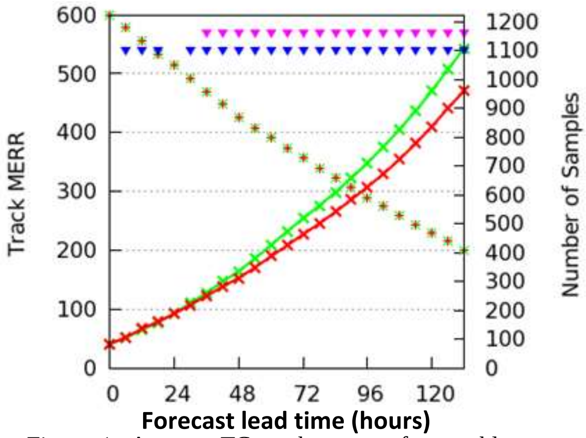

Figure 1: Average TC track errors of ensemble mean forecasts for the western North Pacific region as a function of forecast lead time up to 132 hours. The red and green lines represent positional errors for GEPS and TEPS, respectively. Red plus signs and green x-marks indicate the number of cases included in the statistics. The pink/blue triangles at the top indicate that the difference is statistically significant at the 0.05 level with/without consideration of temporal correlation between the cases.

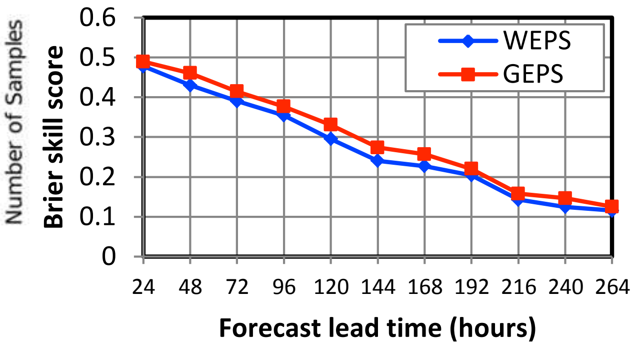

Figure 2: Brier skill scores for probabilistic forecasts of 24-hour cumulative precipitation exceeding 1 mm over Japan during winter 2015/16 as a function of forecast lead time up to 264 hours. The red and blue lines represent verification results for GEPS and WEPS, respectively.

Upgrade of JMA's operational global NWP system

Hitoshi Yonehara, Ryouhei Sekiguchi, Takafumi Kanehama, Kei Saitou, Teppei Kinami,
Akira Shimokobe, Daisuke Hotta, Ryoji Nagasawa, Hitoshi Sato, Masashi Ujiie,
Takashi Kadowaki, Syoukichi Yabu, Kazutaka Yamada, Masayuki Nakagawa,
Takayuki Tokuhiro
Japan Meteorological Agency, Tokyo, Japan
(email: yonehara@met.kishou.go.jp)

1. Introduction

In May 2017, the Japan Meteorological Agency (JMA) upgraded its operational global NWP system by introducing a revised version of its Global Spectral Model (GSM: JMA 2013). The revision involved the refinement of various parametrized processes, including cloud, convection, surface, and radiation schemes, which collectively resulted in forecast improvement. This report outlines each component of the upgrade.

2. Major updates

2.1 Cloud and convection

Melting and re-evaporation processes were revised to address inadequate cooling caused by the artificial limiters applied to evaporation/condensation heating rates in order to ensure stable time integration. The new schemes consist of a rain evaporation scheme (Kessler 1969) with an implicit time discretization method and simple relaxation parameterization to account for melting of snow that falls across the freezing level. These changes induced another cooling bias in the lower troposphere, which was mitigated by refining the convective downdraft treatment to suppress excessive evaporation.

2.2 Land model

The leaf area index (LAI), vegetation cover ratio and soil parameters were updated using more accurate reference sources. The soil moisture content climatology used to initialize the land model is now produced using atmospheric forcing datasets from the Global Soil Wetness Project Phase 3. The LAI data were also updated from more recent satellite observations (Myneni et al. 2002). These updates resulted in reduction of the excessive sensible heat flux seen in the previous model.

2.3 Radiation

Aerosol radiation treatment was refined for separate consideration of the radiative properties of five types of aerosols (sulfate, black carbon, organic carbon, sea salt and mineral dust) to improve representation of their radiative effects (Yabu et al. 2017). A deep cumulus diagnostic scheme was incorporated into the radiation scheme to reduce excessive biases seen in downward short-wave flux at the surface.

2.4 Other changes

A new sea-ice estimation method, updated sea surface temperature climatology data, a revised discretization technique for pressure gradient force, and a stratospheric methane oxidation parameterization based on Untch and Simmons (1999) were adopted. The background error covariance in 4D-Var data assimilation was updated to ensure consistency with the error characteristics of the first guess.

3. Verification results

Twin examinations were conducted to compare forecast scores of the previous and updated systems for two separate periods of July to September (JAS) 2015 and December to February (DJF) 2015/2016. Forecasts were improved overall, with particular enhancement in temperature and wind fields. Figure 1 shows vertical profiles of root mean square errors (RMSEs) for temperature forecasts up to 11 days ahead verified against analysis averaged over the Northern Hemisphere (20 – 90°N) for the JAS period. The upgraded system exhibits reduced RMSEs for most pressure levels and forecast lead times as compared to the previous version (Yonehara et al. 2017). Other forecast elements such as geopotential height and winds were similarly improved.

References

Japan Meteorological Agency, 2013: Outline of Operational Numerical Weather Prediction at JMA. Japan Meteorological Agency, Tokyo, Japan.

Kessler, E., 1969: On the distribution and continuity of water substance in atmospheric circulation. Meteorological Monographs, Vol. 10. Am. Meteorol. Soc., Boston, MA.

Myneni, R. B., S. Hoffman, Y. Knyazikhin, J. L. Privette, J. Glassy, Y. Tian, Y. Wang, X. Song, Y. Zhang, G. R. Smith, A. Lotsch, M. Friedl, J. T. Morisette, P. Votava, R. R. Nemani and S. W. Running, 2002: Global products of vegetation leaf area and fraction absorbed PAR from year one of MODIS data. Remote Sens. Environ., 83, 214 – 231.

Untch, A. and A. J. Simmons, 1999: Increased stratospheric resolution in the ECMWF forecasting system. ECMWF Newsletter, No. 82, 2 – 8.

Yabu, S., T. Y. Tanaka and N. Oshima, 2017: Development of a multi-species aerosol-radiation scheme in JMA's global model. CAS/JSC WGNE Res. Activ. Atmos. Oceanic Modell., 4.15 – 4.16.

Yonehara, H., T. Tokuhiro, R. Nagasawa, M. Ujiie, A. Shimokobe, M. Nakagawa, R. Sekiguchi, T. Kanehama, H. Sato and K. Saitou, 2017: Upgrade of parameterization schemes in JMA's operational global NWP model. CAS/JSC WGNE Res. Activ. Atmos. Oceanic Modell., 4.17 – 4.18.

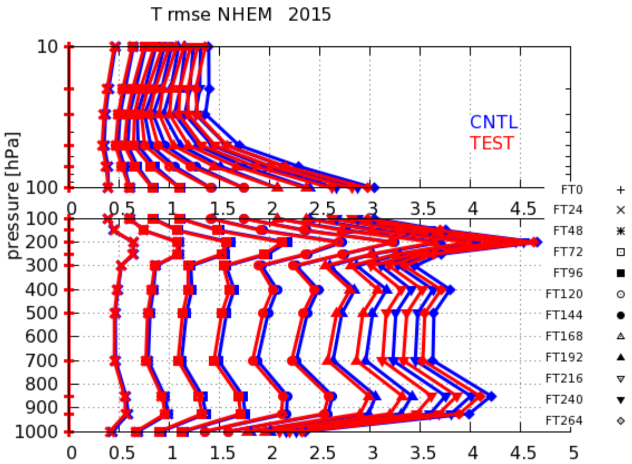

Fig. 1: Profiles of RMSE (CNTL(old)/TEST(new)) for temperature [K]. The reference values are the respective analysis results, and the verification region is the Northern Hemisphere (20 – 90°N). The trial period was 2015JAS. The lines show results for a forecast lead time from FT = 0h to FT = 264h at 24-hour intervals.